Research Article | Vol. 27, No. 6 | 18 Mar 2019 | OPTICS EXPRESS 8335
Optics EXPRESS

Measurement of the relative non-degenerate two-photon absorption cross-section for fluorescence microscopy

SANAZ SADEGH,[1,6,*] MU-HAN YANG,[2,6] CHRISTOPHER G. L. FERRI,[1,6] MARTIN THUNEMANN,[1] PAYAM A. SAISAN,[1] ANNA DEVOR,[1,3,4,7] AND YESHAIAHU FAINMAN[5,7]

[1]*Department of Neurosciences, University of California, San Diego, CA 92093, USA*
[2]*Electrical and Computer Engineering Graduate Program, UCSD, La Jolla, CA 92093, USA*
[3]*Department of Radiology, UCSD, La Jolla, CA 92093, USA*
[4]*Martinos Center for Biomedical Imaging, MGH, Harvard Medical School, Charlestown, MA 02129, USA*
[5]*Department of Electrical and Computer Engineering, UCSD, La Jolla, CA 92093, USA*
[6]*These authors contributed equally to this work*
[7]*These senior authors equally contributed to this study*
[*]*ssadegh@ucsd.edu*

Abstract: In non-degenerate two-photon microscopy (ND-TPM), the required energy for fluorescence excitation occurs via absorption of two photons of different energies derived from two synchronized pulsed laser beams. ND-TPM is a promising imaging technology offering flexibility in the choice of the photon energy for each beam. However, a formalism to quantify the efficiency of two-photon absorption (TPA) under non-degenerate excitation, relative to the resonant degenerate excitation, is missing. Here, we derive this formalism and experimentally validate our prediction for a common fluorophore, fluorescein. An accurate quantification of non-degenerate TPA is important to optimize the choice of photon energies for each fluorophore.

1. Introduction

Fluorescence microscopy is an essential tool in biomedical imaging due to the availability of a wide spectrum of fluorescent dyes and probes [1]. Invention of two-photon microscopy (TPM) pushed the frontiers of fluorescence imaging, enabling high-resolution measurements through hundreds of microns of light-scattering biological tissues [2]. In classical TPM, fluorescence excitation happens via absorption of two photons with the same energy. However, the energies of the two photons do not need to be the same: the sum of their energies must be equal to the total energy required for the ground state to excited state transition. This feature allows for non-degenerate two-photon excitation (ND-TPE), where excitation occurs via simultaneous absorption of two photons of different energies derived from two laser beams. ND-TPE has been exploited in fluorescence microscopy to extend the range of excitation wavelengths [3–5], increase resolution [6, 7], increase penetration depth [8, 9], and mitigate excitation outside of the focal volume [10–13]. Outside of microscopy applications, ND-TPE is also being used in quantum spectroscopy for investigating dipole forbidden transitions [14–17], and in semiconductor optical devices for sensitive infrared detection [18].

Probability of two-photon absorption by a molecule is quantified as the two-photon absorption cross-section (TPACS). A selection criterion for fluorescent probes used in two-photon fluorescence microscopy is to have as large of a TPACS as possible, in order to minimize the excitation power and reduce associated phototoxicity [19]. Therefore, TPACS is a critical property of fluorophores used in biological research [20, 21]. A theoretical framework for quantification of degenerate TPACS (D-TPACS) was developed by Xu and Webb [20]. Their two-photon

#352796 https://doi.org/10.1364/OE.27.008335
Journal © 2019 Received 30 Nov 2018; revised 13 Feb 2019; accepted 13 Feb 2019; published 7 Mar 2019

Optics EXPRESS

spectrometer relies on sensitive detection of the two-photon fluorescence excitation, taking advantage of the high sensitivity of modern photodetectors which can detect single photons as long as the background signal is virtually zero. For non-degenerate TPACS (ND-TPACS), several prior studies employed the Z-scan or pump-probe techniques which measure transmittance [14–17, 22, 23], i.e., a laser intensity decrease due to absorption. However, since TPA is a low probability nonlinear optical process, Z-scan two-photon absorption spectroscopy requires significantly higher laser intensities, compared to two-photon fluorescence excitation spectroscopy, for detecting the inherently low probability two-photon absorption process. The high power requirement of the Z-scan technique is even more problematic for quantification of fluorescent molecules, particularly those used in biological research, which rapidly photobleach under high illumination power. Thus, a more sensitive, low excitation power method for quantification of ND-TPACS is needed.

Toward this end, we extend the two-photon fluorescence excitation technique [20] to allow for ND-TPE. We derive the formalism for the quantifying fluorescence signal generated by ND-TPE of a fluorophore solution illuminated by two ultrashort pulsed lasers. The beams are spatially overlapped, and the fluorescence signal is calculated as a function of the temporal delay between the pulses. We assume that the fluorophore solution is homogeneous, the pulses are transform-limited Gaussian pulses, the excitation beams are undepleted and there is no photobleaching and no saturated absorption. We demonstrate that the ND-TPACS can be calculated from the temporal convolution of the two laser pulses, and that these values can be normalized to the best achievable D-TPACS. The normalization of ND-TPACS values to the corresponding best achievable D-TPACS makes it possible to quantitively compare the ND-TPAC to D-TPACS of the sample and eliminates the necessity for measuring collection efficiency of the system. Finally, we experimentally validate our theoretical prediction: we apply the non-degenerate two-photon fluorescence excitation technique to measure ND-TPACS of a well-characterized fluorophore, fluorescein [20, 21], throughout our available tuning range and compare them to the corresponding D-TPACS. We observe a high correlation between D-TPE and ND-TPE spectra, as expected from the original two-photon excitation theory [24], we also observe that for some wavelength combinations the values of normalized ND-TPACS are larger than D-TPACS, showing enhancement of the TPACS under ND-TPE. We also confirm that the fluorescence generated by ND-TPE is linearly proportional to the excitation power of each beam [8, 25].

2. Theoretical framework

In this section, we extend the formalism given in [20] for fluorescence generated by D-TPE, to allow for ND-TPE in order to derive the relation between fluorescence generated under ND-TPE and the ND-TPAC of the sample. We begin by assuming two pulsed laser beams are chosen within the near infrared window of 700 – 1000 nm and the infrared window of 1000 – 1700 nm, hereafter referred to as the near infrared (NIR) and infrared (IR) beams, respectively. These spectral windows are relevant for ND-TPE spectra of fluorophores that are excitable via D-TPE within the 850 – 1000 nm spectral window. The derivation presented here is more general and would equally apply to any other wavelength combination. When the fluorescent sample is illuminated with the NIR and IR beams that are temporally delayed by offset τ, the number of molecules that are excited via D-TPE and ND-TPE per unit time and unit volume is given by

$$\begin{aligned} N_{\mathrm{ex}}(\boldsymbol{r},t,\tau) = {} & \frac{1}{2}\sigma_{\mathrm{D}}^{(2)}(\lambda_{\mathrm{NIR}})C(\boldsymbol{r},t)I_{\mathrm{NIR}}^{2}(\boldsymbol{r},t-\tau) + \frac{1}{2}\sigma_{\mathrm{D}}^{(2)}(\lambda_{\mathrm{IR}})C(\boldsymbol{r},t)I_{\mathrm{IR}}^{2}(\boldsymbol{r},t) \\ & + 2\sigma_{\mathrm{ND}}^{(2)}(\lambda_{\mathrm{NIR}},\lambda_{\mathrm{IR}})C(\boldsymbol{r},t)I_{\mathrm{NIR}}(\boldsymbol{r},t-\tau)I_{\mathrm{IR}}(\boldsymbol{r},t), \end{aligned} \tag{1}$$

where $\boldsymbol{r} = (x, y)$ is the distance from the optical axis, λ_{NIR} and λ_{IR} are the wavelengths of the NIR and IR beams, $C(\boldsymbol{r}, t)$ is the space- and time-dependent distribution of the fluorophore

Optics EXPRESS

concentration, I_{NIR} and I_{IR} are the space- and time-dependent photon fluxes of each beam (in $\mathrm{cm}^{-2}\mathrm{s}^{-1}$), $\sigma_{\mathrm{D}}^{(2)}(\lambda_{\mathrm{i}})$ and $\sigma_{\mathrm{ND}}^{(2)}(\lambda_{\mathrm{i}}, \lambda_{\mathrm{j}})$ are the D-TPACS and ND-TPACS. Note that the ND-TPACS and D-TPACS become equivalent when two wavelengths are equal, $\sigma_{\mathrm{ND}}^{(2)}(\lambda_{\mathrm{i}}, \lambda_{\mathrm{j}}) = \sigma_{\mathrm{D}}^{(2)}(\lambda_{\mathrm{i}})$ [17]. We assume that both the NIR and IR excitation beams are undepleted for all time and relative pulse delays. The factor of $1/2$ in front of the first two terms of Eq. (1) reflects the fact that in the D-TPE process two photons of the same color are needed to excite one molecule [20]. There is no factor of $1/2$ in front of the last term because in every non-degenerate absorption process only one photon of each color is needed to excite one molecule [18], and the additional factor of 2 in front of the last term comes from the fact that the two absorbed photons are distinguishable while $\sigma_{\mathrm{ND}}^{(2)}(\lambda_{\mathrm{NIR}}, \lambda_{\mathrm{IR}}) = \sigma_{\mathrm{ND}}^{(2)}(\lambda_{\mathrm{IR}}, \lambda_{\mathrm{NIR}})$ [25,26].

We approximate each beam as a Gaussian pulse with a Gaussian cross section in the paraxial approximation, which allows us to separate the temporal and spatial components of the photon flux:

$$I_{\mathrm{IR}}(\boldsymbol{r}, t) = S(\boldsymbol{r}; \lambda_{\mathrm{IR}}) T(t; \lambda_{\mathrm{IR}}) \tag{2}$$

$$I_{\mathrm{NIR}}(\boldsymbol{r}, t, \tau) = S(\boldsymbol{r}; \lambda_{\mathrm{NIR}}) T(t - \tau; \lambda_{\mathrm{NIR}}), \tag{3}$$

where the foci of NIR and IR beams are assumed to be overlapped in space, and

$$T(t; \lambda) = I_0^{(\lambda)} \exp\left(\frac{-t^2}{2\Gamma_\lambda^2}\right) \tag{4}$$

$$S(\boldsymbol{r}; \lambda) = \left[\frac{w_0(\lambda)}{w(z; \lambda)}\right]^2 \exp\left[-2\left(\frac{r}{w(z; \lambda)}\right)^2\right]. \tag{5}$$

The pulsed beams are assumed to have transform-limited pulses with peak photon flux density $I_0^{(\lambda)}$ (in $\mathrm{cm}^{-2}\mathrm{s}^{-1}$) and temporal standard deviation Γ_λ, and

$$w^2(z; \lambda) = w_0^2(\lambda)\left[1 + \left(\frac{z}{z_0(\lambda)}\right)^2\right], \quad z_0(\lambda) = \frac{\pi w_0^2(\lambda)}{\lambda}, \quad w_0(\lambda) = \frac{\lambda}{\pi \mathrm{NA}}, \tag{6}$$

where $w_0(\lambda)$ is the beam waist, $z_0(\lambda)$ is the Rayleigh length and NA is the numerical aperture of the optical system. Inserting these expressions into Eq. (1) and separating the spatial and temporal terms we find that the number of excited molecules per unit time in the illuminated sample volume, V, is given by

$$\begin{aligned} N_{\mathrm{ex}}(t, \tau) = {} & \sigma_{\mathrm{D}}^{(2)}(\lambda_{\mathrm{NIR}}) C T^2(t - \tau; \lambda_{\mathrm{NIR}}) \int_V \mathrm{d}V [S(\boldsymbol{r}; \lambda_{\mathrm{NIR}})]^2 \\ & + \sigma_{\mathrm{D}}^{(2)}(\lambda_{\mathrm{IR}}) C T^2(t; \lambda_{\mathrm{IR}}) \int_V \mathrm{d}V [S(\boldsymbol{r}; \lambda_{\mathrm{IR}})]^2 \\ & + \sigma_{\mathrm{ND}}^{(2)}(\lambda_{\mathrm{NIR}}, \lambda_{\mathrm{IR}}) C T(t; \lambda_{\mathrm{IR}}) T(t - \tau; \lambda_{\mathrm{NIR}}) \int_V \mathrm{d}V S(\boldsymbol{r}; \lambda_{\mathrm{IR}}) S(\boldsymbol{r}; \lambda_{\mathrm{NIR}}). \end{aligned} \tag{7}$$

We assume that the fluorophores are distributed homogeneously and are stable over the course of each measurement, i.e., $C(\boldsymbol{r}, t) = C$, and can therefore be moved in front of the integrals. By assuming the fluorescence spot size is much smaller than the volume of the fluorophore solution

and that numerical apertures of the beams are roughly equal, we find that for the general case of two beams with wavelengths λ_1 and λ_2 the spatial overlap integral is

$$\int_V \mathrm{d}V S(\boldsymbol{r};\lambda_1)S(\boldsymbol{r};\lambda_2) = \frac{(\lambda_1\lambda_2)^2}{2\sqrt{2}\pi \mathrm{NA}^4\sqrt{\lambda_1^2+\lambda_2^2}}. \tag{8}$$

For the degenerate case, the wavelengths are equal, $\lambda_1 = \lambda_2 = \lambda_{\mathrm{NIR}}$ or λ_{IR}, and the spatial overlap integral result simplifies to $\lambda^3\backslash\left(4\pi\mathrm{NA}^4\right)$. For the non-degenerate case, $\lambda_1 = \lambda_{\mathrm{IR}}$ and $\lambda_2 = \lambda_{\mathrm{NIR}}$.

To relate the fluorescence photon flux to N_{ex}, we follow Xu and Webb [20]: assuming no stimulated emission, photo-bleaching or saturated absorption, the fluorescence photon flux is

$$F(t,\tau) = \phi\eta N_{\mathrm{ex}}(t,\tau), \tag{9}$$

where ϕ is the collection efficiency of the optical system, and η is the fluorescence quantum efficiency. Substituting Eq. (7) and Eq. (8) into Eq. (9) we find the following expression for the fluorescence photon flux

$$\begin{aligned} F(t,\tau) = &\frac{\phi\eta\sigma_{\mathrm{D}}^{(2)}(\lambda_{\mathrm{NIR}})C\lambda_{\mathrm{NIR}}^3 T^2(t-\tau;\lambda_{\mathrm{NIR}})}{8\pi\mathrm{NA}^4} + \frac{\phi\eta\sigma_{\mathrm{D}}^{(2)}(\lambda_{\mathrm{IR}})C\lambda_{\mathrm{IR}}^3 T^2(t;\lambda_{\mathrm{IR}})}{8\pi\mathrm{NA}^4} \\ &+ \frac{\phi\eta\sigma_{\mathrm{ND}}^{(2)}(\lambda_{\mathrm{NIR}},\lambda_{\mathrm{IR}})C\lambda_{\mathrm{NIR}}^2\lambda_{\mathrm{IR}}^2 T(t-\tau;\lambda_{\mathrm{NIR}})T(t;\lambda_{\mathrm{IR}})}{\sqrt{2}\pi\mathrm{NA}^4\sqrt{\lambda_{\mathrm{NIR}}^2+\lambda_{\mathrm{IR}}^2}}. \end{aligned} \tag{10}$$

We recognize that the signal measured by our fluorescence detector is the time averaged photon flux, not the instantaneous photon flux; as a result, we need to compute the time average of Eq. (10). To compute the time average, we solve the time overlap integral for the general case with two wavelengths λ_1 and λ_2 and non-zero temporal offset:

$$\langle T(t;\lambda_1)T(t-\tau;\lambda_2)\rangle = f\int_{-\frac{1}{2f}}^{\frac{1}{2f}} \mathrm{d}t' T(t';\lambda_1)T(t'-\tau;\lambda_2), \tag{11}$$

where f is laser repetition rate. If we assume pulse width and delay time are much smaller than $1/f$, which is valid for an 80 MHz femtosecond pulsed laser, we can approximate the limits of the time overlap integral to be infinite:

$$\int_{-\frac{1}{2f}}^{\frac{1}{2f}} \mathrm{d}t' T(t';\lambda_1)T(t'-\tau;\lambda_2) \approx \int_{-\infty}^{\infty} \mathrm{d}t' T(t';\lambda_1)T(t'-\tau;\lambda_2). \tag{12}$$

This expression is equivalent to the temporal convolution of our laser pulses. By substituting Eq. (4) into Eq. (12) we see that as a function of delay time, we have the convolution of two Gaussian functions, which is typically computed by application of the convolution theorem:

$$h * g = \mathcal{F}^{-1}\left\{\mathcal{F}\{h\}\cdot\mathcal{F}\{g\}\right\}, \tag{13}$$

where $h * g$ denotes the convolution of functions h and g and $\mathcal{F}\{\}$ is the Fourier transform. Therefore, the temporal convolution of the Gaussian pulses is

$$\int_{-\infty}^{\infty} \mathrm{d}t' I_0^{(\lambda_1)} I_0^{(\lambda_2)} \exp\left(\frac{-(t'-\tau)^2}{2\Gamma_{\lambda_1}^2}\right)\exp\left(\frac{-t'^2}{2\Gamma_{\lambda_2}^2}\right) = \sqrt{2\pi} I_0^{(\lambda_1)} I_0^{(\lambda_2)} \frac{\Gamma_{\lambda_1}\Gamma_{\lambda_2}}{\Gamma_x}\exp\left(\frac{-\tau^2}{2\Gamma_x^2}\right), \tag{14}$$

where $\Gamma_x^2 = \Gamma_{\lambda_1}^2 + \Gamma_{\lambda_2}^2$ is the standard deviation of the convolution. For the degenerate case, wavelengths, temporal standard deviations, and peak photon flux densities are equal and $\tau = 0$, therefore, the temporal overlap integral simplifies to $\pi I_0^2 \Gamma$.

To complete the derivation, we rewrite the time-averaged fluorescence in terms of the average laser power measured with a power meter (in mW). Because we assumed transform limited pulses with a Gaussian spatial profile, we can write the power in terms of the photon flux

$$\langle P_\lambda \rangle = I_T E_\lambda f, \tag{15}$$

where $I_T = \iiint_{-\infty}^{\infty} I_\lambda(x,y,t)dxdydt = I_0^{(\lambda)}\sqrt{\pi^3/2}\Gamma_\lambda w_0^2$ is the total photon flux at the focus, and E_λ is the energy per photon. Consequently, we obtain the following equation for the laser photon flux

$$I_0^{(\lambda)} = \frac{2\lambda\langle P_\lambda\rangle}{\pi\sqrt{2\pi}\Gamma_\lambda chf w_0^2} = \frac{\sqrt{2\pi}\mathrm{NA}^2\langle \mathrm{P}_\lambda\rangle}{\Gamma_\lambda chf\lambda} \tag{16}$$

where c is the speed of light, and h is Plank's constant. Therefore, assuming: the fluorophore solution is homogeneous; the paraxial beam approximation; an approximately constant numerical aperture; transform limited Gaussian pulses; and, undepleted excitation beams, the time averaged fluorescence as a function of relative pulse delay is

$$\begin{aligned}\langle F(\tau)\rangle = &\frac{\sqrt{\pi}C\langle P_{\mathrm{NIR}}\rangle^2\lambda_{\mathrm{NIR}}\phi\eta\sigma_{\mathrm{D}}^{(2)}(\lambda_{\mathrm{NIR}})}{4fc^2h^2\Gamma_{\mathrm{NIR}}} + \frac{\sqrt{\pi}C\langle P_{\mathrm{IR}}\rangle^2\lambda_{\mathrm{IR}}\phi\eta\sigma_{\mathrm{D}}^{(2)}(\lambda_{\mathrm{IR}})}{4fc^2h^2\Gamma_{\mathrm{IR}}} \\ &+ \frac{2\sqrt{\pi}C\langle P_{\mathrm{NIR}}\rangle\langle P_{\mathrm{IR}}\rangle\lambda_{\mathrm{NIR}}\lambda_{\mathrm{IR}}\phi\eta\sigma_{\mathrm{ND}}^{(2)}(\lambda_{\mathrm{NIR}},\lambda_{\mathrm{IR}})}{fc^2h^2\Gamma_x\sqrt{\lambda_{\mathrm{NIR}}^2+\lambda_{\mathrm{IR}}^2}}\exp\left(\frac{-\tau^2}{2\Gamma_x^2}\right).\end{aligned} \tag{17}$$

The first two terms of Eq. (17) are the fluorescence from D-TPE which is constant as a function of pulse delay and appear as a constant fluorescence background. By acquiring the fluorescence intensity as a function of relative pulse delay, we can measure both the ND-TPACS and D-TPACS by fitting this model to the data, assuming that all other parameters including the fluorophore concentration, fluorescence quantum efficiency and collection efficiency are known. Note that for the limit that $\lambda_{\mathrm{NIR}} = \lambda_{\mathrm{IR}}$, our setup becomes an interferometric autocorrelator, see Appendix E, and the measured fluorescence is the interferometric autocorrelator trace [27] which is very sensitive to the optical path difference between the two beams.

As described above, measurement of the absolute ND-TPACS would require knowledge of the fluorophore quantum efficiency η and the collection efficiency of the measurement system ϕ. Our goal, however, is to compare ND-TPACS to the corresponding D-TPACS. Therefore, we calculate the ratio of the maximum non-degenerate two-photon excited fluorescence ($\tau = 0$) to the degenerate two-photon excited fluorescence at a chosen wavelength, λ_{D}, given by

$$\frac{\langle F(\tau=0)\rangle_{\mathrm{ND}(\lambda_{\mathrm{NIR}},\lambda_{\mathrm{IR}})}}{\langle F\rangle_{\mathrm{D}(\lambda_{\mathrm{D}})}} = 8\frac{\langle P_{\mathrm{NIR}}\rangle\langle P_{\mathrm{IR}}\rangle\lambda_{\mathrm{NIR}}\lambda_{\mathrm{IR}}\sigma_{\mathrm{ND}}^{(2)}(\lambda_{\mathrm{NIR}},\lambda_{\mathrm{IR}})\Gamma_{\mathrm{D}}}{\Gamma_x\langle P_{\mathrm{D}}\rangle^2\lambda_{\mathrm{D}}\sigma_{\mathrm{D}}^{(2)}(\lambda_{\mathrm{D}})\sqrt{\lambda_{\mathrm{NIR}}^2+\lambda_{\mathrm{IR}}^2}}, \tag{18}$$

consequently, the ND-TPACS that is normalized by D-TPACS at wavelength λ_{D} is

$$\frac{\sigma_{\mathrm{ND}}^{(2)}(\lambda_{\mathrm{NIR}},\lambda_{\mathrm{IR}})}{\sigma_{\mathrm{D}}^{(2)}(\lambda_{\mathrm{D}})} = \frac{\lambda_{\mathrm{D}}\sqrt{\lambda_{\mathrm{NIR}}^2+\lambda_{\mathrm{IR}}^2}\Gamma_x\langle P_{\mathrm{D}}\rangle^2\langle F(\tau=0)\rangle_{\mathrm{ND}(\lambda_{\mathrm{NIR}},\lambda_{\mathrm{IR}})}}{8\lambda_{\mathrm{NIR}}\lambda_{\mathrm{IR}}\Gamma_{\mathrm{D}}\langle P_{\mathrm{NIR}}\rangle\langle P_{\mathrm{IR}}\rangle\langle F\rangle_{\mathrm{D}(\lambda_{\mathrm{D}})}} \tag{19}$$

Optics EXPRESS

Our normalization procedure assists us with quantifying the ND-TPACS relative to the best achievable D-TPACS of the same fluorophore and does not rely on previously published D-TPACS of reference fluorophores.

3. Experimental validation

3.1. Sample preparation

Fluorescein (SIGMA-ALDRICH) was dissolved in 1X phosphate-buffered saline to reach ~ 100 μM concentration. The pH of the solution was measured after dissolving the fluorescein (pH ~ 7.4). The true concentration, 88 μM, was measured using single-photon absorption spectroscopy (NanoDrop 2000 spectrometer, ThermoFisher) and previously published molar extinction coefficient (75000 M^{-1} cm^{-1}).

3.2. Experimental apparatus

Figure 1 depicts the experimental setup for ND-TPACS measurements using the non-degenerate two-photon fluorescence excitation technique. The primary light source was a Coherent Chameleon Ultra II laser, which generates 140 – 190 fs pulses with an 80 MHz repetition rate in the 680 – 1080 nm spectral range and is referred as the NIR beam. The Chameleon was used to pump an APE Chameleon Compact Optical Parametric Oscillator (OPO), which has a signal tuning range of 1000 – 1600 nm (referred as the IR beam). Since the OPO could only be pumped with an NIR beam within the 740 – 880 nm range, the actual available tuning range of the NIR beam for simultaneous sample excitation with NIR and IR beams is smaller than the entire tuning range of the Chameleon Ultra II laser. A built-in bypass beam splitter diverted 15% of the NIR beam to be used as one of the fluorescence excitation beams. The second beam was the signal from the OPO. The power of each beam was controlled using a half wave plate/linear polarizer combination and monitored using an uncoated quartz glass slide (for beam sampling) and a power meter (Melles Griot, broadband power meter, 13PEM001) during the experiment. The laser power after the objective was measured for each wavelength and a table for the ratio of the powers measured in the setup and power after objective was generated, in other words, the transmission spectrum of the optical path after the beam sampler was measured for each laser. This was a necessary step since the transmittance of optical elements are slightly different for different wavelengths. The path length difference between the two beams was tuned using a custom optical delay line in the NIR path, which utilized a Thorlabs LTS150 150 mm linear translation stage with repeatable incremental motion of 2 μm, corresponding to a minimum time delay resolution of 13 fs. Both beams were expanded to overfill the microscope objective pupil aperture and co-polarized using halfwave plates. Subsequently, the two beams were combined and made collinear using a dichroic beam splitter with a cutoff wavelength at 1000 nm (Thorlabs, DMSP 1000). See Appendix A for a note on beam alignment. The resulting combined beam was then directed into the microscope objective (Olympus, LMPLN-10X-IR, NA=0.3), which focused the beam into a rectangular Quartz cuvette (WPI, 2 mm path, 0.7 mL volume) filled with sample solution.

The emission was collected in epi-fluorescence mode, reflected off two dichroic mirrors with cutoffs of 678 nm (Semrock, FF678-Di01-25x36) and 735 nm (Semrock, FF735-Di01-25x36) and subsequently passed through a set of fluorescence bandpass filters (three Semrock FF01-550/200-25 and one Semrock FF01-525/50-25) to extinguish the excitation source and lower the scattered pump signal below the electronic noise in the collection path. Finally, the fluorescence was detected using a photomultiplier (PMT; Hamamatsu, H11461-03). We verified that the fluorescence emission spectrum is identical under ND-TPE and D-TPE (Appendix B), and therefore the collection path does not need to change for these two types of excitation. The PMT signal was amplified by a transimpedance amplifier (Hamamtsu C9999). The signal from

Optics EXPRESS

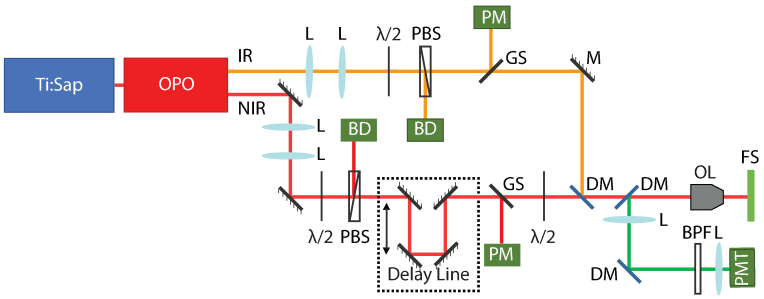

Fig. 1. Experimental setup for demonstration of non-degenerate two-photon fluorescence excitation technique. L, lens; PBS, polarizing beam splitter; $\lambda/2$, half wave plate; GS, glass slide; M, mirror; DM, dichroic mirror; BD, beam dump; FS, fluorescent sample; OL, objective lens; BPF, band pass filter; PM, power meter; PMT, photomultiplier.

the amplifier and the laser power meter readings were acquired using a data acquisition board (National Instruments). Data acquisition and analysis were performed using custom-written software (National Instruments, LabVIEW). Please see Appendix C for the spectroscopy protocol.

3.3. *Experimental results*

The fluorescence intensity of fluorescein was measured as a function of the temporal delay between the excitation pulses, resulting in a signal which was dependent on the temporal convolution between the NIR and IR pulses (Fig. 2(a)). The NIR laser beam generated degenerate two-photon fluorescence which appeared as a constant fluorescence background upon which the convolution signal from ND-TPE was added (Eq. (17)). For the selected tuning range, the contribution of the IR to D-TPE was insignificant relative to the NIR beam contribution, because of the extremely low D-TPACSs in this range. The fluorescence intensity curves, i.e., the convolution signals, were generated for each combination of NIR and IR wavelengths with 740 nm $< \lambda_{NIR} <$ 870 nm and 1030 nm $< \lambda_{IR} <$ 1400 nm, producing a 2-dimensional ND-TPACS spectrum. The ND-TPACS was extracted from the convolution signal as described in previous sections. We can normalize ND-TPACS spectra to any spectral feature of interest. We chose to normalize the ND-TPACS data by the peak D-TPACS at $\lambda_{NIR} = 920$ nm, meaning that we normalized ND-TPACS by the corresponding best achievable D-TPACS for the given fluorophore. The resulting normalized 2-dimensional ND-TPACS spectrum is shown in Fig. 2(b). For some of the wavelength combinations, less than 5% of points, the convolution curve significantly deviated from the predicted Gaussian profile. For these data points, we chose to interpolate the data, please refer to Appendix D for details. As expected, the highest fluorescence flux was obtained when the sum of NIR and IR photon energies matched the transition energy. In Fig. 2(b), the isocline corresponding to a transition energy of 2.7 eV, corresponding to the 920 nm peak in the D-TPE spectrum of fluorescein, is overlaid on the fluorescein ND-TPE spectrum.

In Fig. 2(c) we show the normalized ND-TPACS spectra plotted versus the degenerate wavelength equivalent to every combination of IR and NIR wavelengths used to excite the sample, i.e., $2/\lambda_{Eq} = 1/\lambda_{NIR} + 1/\lambda_{IR}$. Since all NIR and IR wavelength combinations along one specific isocline correspond to the same equivalent wavelength, we report several ND-TPAC values for each equivalent wavelength. Therefore, variation of ND-TPACS for each equivalent wavelength is not caused by measurement errors as each point represents an individual measurement at a different wavelength combination.

We measured the D-TPACS using two methods: either by blocking the IR beam and illuminating the sample with the NIR beam (independent measurement) or by using the baseline offset of the convolution signal (dependent measurement); please refer to Appendix C for details.

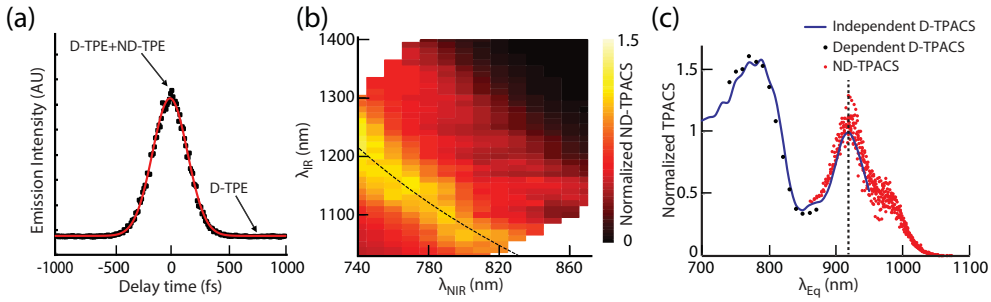

Fig. 2. Non-degenerate two-photon fluorescence excitation spectroscopy of fluorescein. a) A typical plot of fluorescence intensity as a function of the delay time between NIR and IR pulses. The increase in the signal at delays approaching zero is due to ND-TPE. The red line shows the fitted model (Eq. (17)). b) Color-coded ND-TPACS spectrum normalized by the D-TPACS peak at 920 nm, extracted from independent measurements of fluorescein D-TPACS, for fluorescein showing dependence of the ND-TPACS on NIR and IR wavelengths. The 2.7 eV isocline is overlaid as black dashed line. c) Normalized ND-TPACS of fluorescein, as a function of the equivalent degenerate wavelength λ_{Eq} where $2/\lambda_{\mathrm{Eq}} = 1/\lambda_{\mathrm{NIR}} + 1/\lambda_{\mathrm{IR}}$ is shown in red circles. Since all NIR and IR wavelength combinations along one specific isocline in panel b correspond to the same equivalent wavelength, we report several ND-TPAC values for each equivalent wavelength. Independently measured D-TPACS normalized by its peak value at 920 nm is shown as blue line. Dependent D-TPACS extracted from the fluorescence intensity curve background (see panel a) and normalized by the peak value of independently measured D-TPACS at 920 nm is shown in black circles. The dashed line shows the position of the peak at 920 nm.

We normalized both dependent and independent D-TPACS by the independent D-TPACS at $\lambda_{\mathrm{NIR}} = 920$ nm. We also overlay the ND-TPACS spectra with both dependent and independently measured D-TPACS of the dye. We observe that the dependent and independent D-TPACS measurements agree (Fig. 2(c)), which verifies the integrity of the ND-TPACS spectrum. We also see that the shape of the linearized ND-TPACS spectra is highly correlated with the D-TPACS spectra. We observe that for almost all wavelength combinations, the ND-TPACS are larger than the equivalent D-TPACS. This observation is explained by the phenomenon known as "resonance enhancement" [17]: the increased probability of ND-TPE caused by a longer virtual state lifetime as compared to degenerate two-photon excitation.

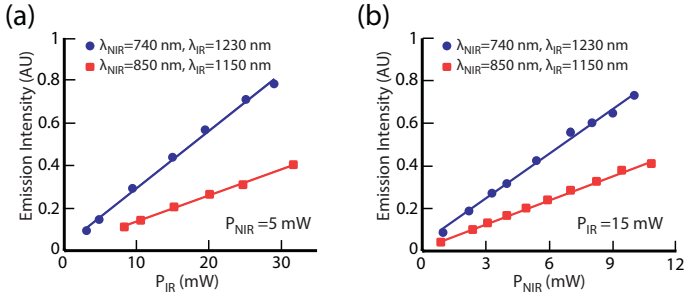

Fig. 3. Non-degenerate two-photon fluorescence excitation dependence on a) IR excitation power ($P_{\mathrm{NIR}} = 5$ mW), and b) NIR excitation power ($P_{\mathrm{IR}} = 15$ mW). The power dependence was tested for two different wavelength combinations: $\lambda_{\mathrm{NIR}} = 740$ nm, $\lambda_{\mathrm{IR}} = 1230$ nm and $\lambda_{\mathrm{NIR}} = 850$ nm, $\lambda_{\mathrm{IR}} = 1150$ nm.

Optics EXPRESS

For both D-TPE and ND-2PE measurements, the laser powers were kept below 30 mW for the IR laser and 10 mW for the NIR laser. In our experimental setup, 1 mW of average excitation power corresponds to $\sim 10^{28}$ photon/(cm^{2}s) laser photon flux. Xu and Webb [20] have demonstrated that for this excitation intensity range, the degenerate two-photon excited fluorescence signal is merely generated by D-TPE and other non-linear phenomena such as stimulated emission and excited-state absorption are absent. From Eq. (17) we expect that the fluorescence generated by ND-TPE scales linearly with excitation power of each beam [8, 13]. To verify that for ND-TPE the generated fluorescent signal is solely due to ND-TPE, we tested the linear power dependence of the generated fluorescence on each laser power for the applied excitation power range for multiple wavelength combinations (Fig. 3). We observe that for both NIR and IR beams the fluorescence caused by ND-TPE is linearly scaled with excitation power of each beam. This behavior is observed for all wavelength combinations where we show two of them in Fig. 3, verifying the assumptions of our model.

4. Conclusion

We reported the theoretical and experimental details of the non-degenerate two-photon fluorescence excitation technique for sensitive measurement of ND-TPACS. Assuming a homogeneous fluorophore solution, the paraxial beam approximation, an approximately constant numerical aperture, transform limited Gaussian pulses, and undepleted excitation beams, we calculated the time averaged fluorescence signal as a function of relative pulse delay. By doing this, we have extended the previously published theoretical framework for fluorescence generated under D-TPE [20] to account for ND-TPE. Using two femtosecond pulsed, synchronized independently tunable lasers, we measured the non-degenerate two-photon excitation spectra of fluorescein. We observe that the shape of the ND-TPE spectrum closely follows that of the D-TPE spectrum. We also found that the ND-TPACs are consistently higher than the D-TPACs for equivalent excitation energies. This enhancement in absorption probability is consistent with the resonance enhancement phenomenon [17]. We demonstrated that within the employed range of laser powers used for the non-degenerate two-photon fluorescence excitation technique, the generated fluorescence scales linearly with the excitation power of each beam showing that the ND-TPE is the only mechanism generating the fluorescence. By introducing the sensitive method for ND-TPACS measurement of fluorescent molecules, we hope to assist future studies on application of ND-TPE in fluorescence microscopy.

Appendix A: Beam size and alignment characterization

The NIR and IR beams were aligned by maximizing the signal generated by a fluorescent sample: steering mirrors were used for in-plane alignment; a telescope was used for axial alignment; a delay line was used for temporal alignment. In order to confirm the beam overlap in space when aligned using the described method, we performed knife-edge beam profiling. In Fig. 4 we show the profiles of NIR, $\lambda_{\mathrm{NIR}} = 740$ nm, and IR, $\lambda_{\mathrm{IR}} = 1230$ nm, beams for three different axial positions ($z = 41, 42, 43$ mm). We fit the measured data by the equation

$$P = P_0 + \frac{1}{2}\left(1 - \mathrm{erf}\left(\frac{\sqrt{2}(x - x_0)}{w}\right)\right), \tag{20}$$

where P is the normalized power, P_0 is the background power, and erf is a standard error function; we obtain a value for the beam radius w and center x_0 for each measured profile. We find that the center of the two beams are aligned almost perfectly in all three transverse planes for both NIR and IR beams ($x_0 = 6.5 \pm 0.1$ mm). The relationship between beam radius and the distance from beam waist z_1 is given by

$$w = w_0\sqrt{1+\left(\frac{z-z_1}{z_0}\right)^2}, \tag{21}$$

where w_0 is the beam waist and z_0 is the Rayleigh range. By using the known w values for the three z positions, we can obtain the z_1, z_0, and w_0 values of each beam. For NIR beam we find $w_0 = 0.7 \pm 0.1$ µm, $z_0 = 1.8 \pm 0.1$ µm, $z_1 = 27.8 \pm 0.5$ mm, and for the IR beam $w_0 = 1.2 \pm 0.1$ µm, $z_0 = 3.8 \pm 0.1$ µm, $z_1 = 27 \pm 0.5$ mm , which indicates that the beams are aligned in the axial direction. Furthermore, from the obtained numbers we see that the $w_0 = \lambda/(\pi \mathrm{NA})$ and $z_0 = \pi w_0^2/\lambda$ relations are valid for the beams that overfill the back aperture of an objective lens with numerical aperture NA. We also confirm the validity of our assumption of constant NA for different wavelengths (NA $= 0.34 \pm 0.1$ for $\lambda_{\mathrm{NIR}} = 740$ nm and NA $= 0.33 \pm 0.1$ for $\lambda_{\mathrm{IR}} = 1230$ nm).

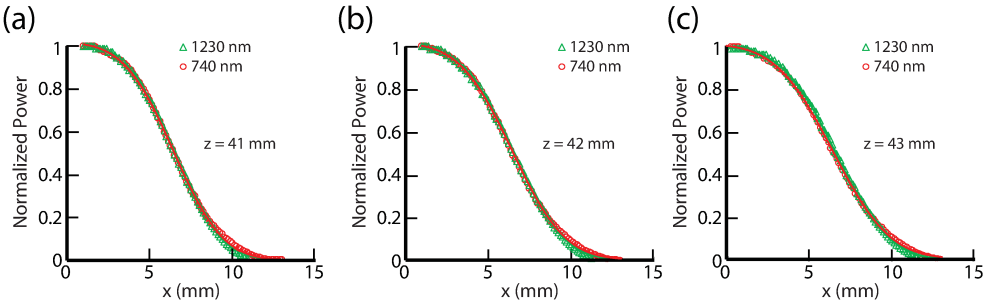

Fig. 4. Beam profiles obtained by knife edge measurement for NIR, $\lambda_{\mathrm{NIR}} = 740$ nm, and IR,$\lambda_{\mathrm{IR}} = 1230$ nm, beams for axial positions a) $z = 41$ mm, b) $z = 42$ mm and c) $z = 43$ mm. The solid lines are the fits of Eq. (20) to the measured data.

Appendix B: Fluorescence emission spectra under ND-TPE and D-TPE

It has been shown that fluorescence generated by single-photon excitation and D-TPE has the same emission spectrum [20]. For fluorescence emission spectrum measurements under D-TPE and ND-TPE, we added a spectrometer (HR4000CG High Resolution Fiber Optic Spectrometer) to the collection path of the setup depicted in Fig. 1. As shown in Fig. 5, we observe that the fluorescence emission spectra under ND-TPE and D-TPE are identical.

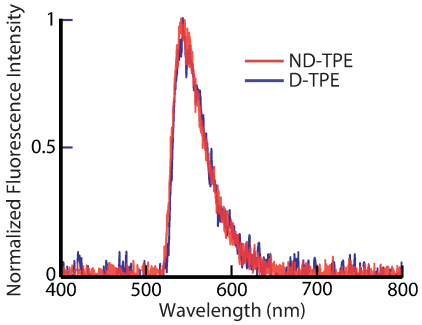

Fig. 5. Fluorescence emission spectra of Fluorescein generated by ND-TPE ($\lambda_{\mathrm{NIR}} = 740$ nm, $\lambda_{\mathrm{IR}} = 1230$ nm) and D-TPE ($\lambda_{\mathrm{NIR}} = 920$ nm).

Optics EXPRESS

Appendix C: Spectroscopy protocol

D-TPACS was acquired by only allowing one laser to illuminate the sample, by using the shutters provided in the OPO to block the unused beam. We then tuned the illumination beam through the desired tuning range in 10-nm steps, which corresponds to the spectral bandwidth of these lasers (5 − 15 nm). At each step we averaged 1000 samples from the PMT and 100 readings from the laser reference power meter, in addition we collected laser repetition rate, wavelength and spectral bandwidth, which were reported by the OPO for each beam. We assumed a transfer-limited Gaussian pulse and calculated the pulse duration, Γ_{NIR}, from the spectral bandwidth that was reported by the OPO. We additionally measured the pulse duration of the NIR beam using frequency-resolved optical gating (GRENOUILLE, Swamp Optics) and confirmed that the transfer limited pulse assumption is valid for our NIR beam. We then used the first term of Eq. (17) to calculate the D-TPACS as a function of collection efficiency and quantum efficiency. We use these independently measured D-TPAC as a calibration for the ND-TPAC data.

ND-TPACS was collected by illuminating the fluorophore solution with the NIR and IR beams simultaneously. To distinguish ND-TPE emission from D-TPE emission, we scanned the relative time delay between the two lasers in 10-fs steps. At each time delay step, fluorescence intensity, laser wavelengths, spectral bandwidths, reference powers and repetition rate were recorded. In addition to the convolution signal, there exists a constant background offset resulting from any D-TPE fluorescence, which is typically generated by the NIR laser (for the selected wavelength combinations). For the selected tuning range, the contribution of the IR beam to D-TPE was lower than the noise level of our PMT, because of the extremely low D-TPACSs in this range. As a result, the model used to fit the convolution data is the sum of a D-2PE offset added to the ND-2PE convolution (Eq. (17)). Therefore, we can measure both D-TPACS and ND-TPACS by fitting the convolution signal to Eq. (17). In our fitting procedure, the fitting parameters where ND-TPACS, D-TPACS at λ_{NIR}, and the standard deviation of the convolution signal Γ_x. We call the D-TPACS measured from fitting the model to the convolution signal the dependently measured D-TPACS or dependent D-TPACS. We then normalized the ND-TPACS and dependently measured D-TPACS to the peak of the independently measured D-TPACS at $\lambda_{\mathrm{NIR}} = 920$ nm. The normalization process eliminates the necessity for measuring the collection efficiency of the system and fluorophore quantum efficiency and concentration. From repeated measurements along the isocline and error propagation analysis we deduced that the relative error in our TPACS measurements is below 15%.

Appendix D: Double peak effect and data interpolation

For some NIR and IR wavelength combinations the fluorescence intensity versus delay time plot significantly deviates from Gaussian profile because of a "double peak" effect that happens in the OPO for that specific wavelength combination. In Fig. 6(a) we show an example of the double peak behavior for one wavelength combination. These points consist less than 5% of the data. We removed these points from our results and linearly interpolated the neighboring data points to fill out the removed data points. Figures 6(b) and 6(c) show the 2-dimensional excitation map of fluorescein before and after data interpolation.

Appendix E: $\lambda_{\mathrm{NIR}} = \lambda_{\mathrm{IR}}$ limit: interferometric autocorrelator

In this section we discuss the limit of $\lambda_{\mathrm{NIR}} = \lambda_{\mathrm{IR}}$ in our experimental setup for ND-TPACS measurement. To mimic our two-beam setup, we split the NIR beam, $\lambda_{\mathrm{NIR}} = 920$ nm, to two beams using a 50 : 50 beam splitter and put one of the beams through the delay line and then combine the beams again before the objective lens as depicted in Fig. 7(a). The resulting setup is an interferometric autocorrelator and the generated fluorescence signal, Fig. 7(b), is an interferometric autocorrelation trace as expected [27].

Optics EXPRESS

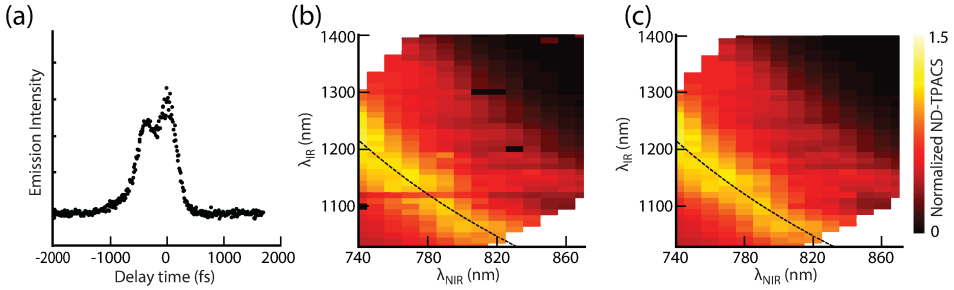

Fig. 6. Data interpolation. a) Fluorescence intensity versus delay time between IR and NIR pulses where λ_{NIR} = 740 nm and λ_{IR} = 1100 nm. The "double peak" effect caused by irregular IR beam profile is clear in the plot. b) Color-coded ND-TPE spectrum normalized to the corresponding D-TPACs at λ_{Eq} = 920 nm, for fluorescein before the interpolation process. c) Same normalized spectrum shown in panel b after removing the "double peak" data points and interpolating the data. The 2.7 eV (λ_{Eq} = 920 nm) isocline is overlaid as black dashed line in (b) and (c).

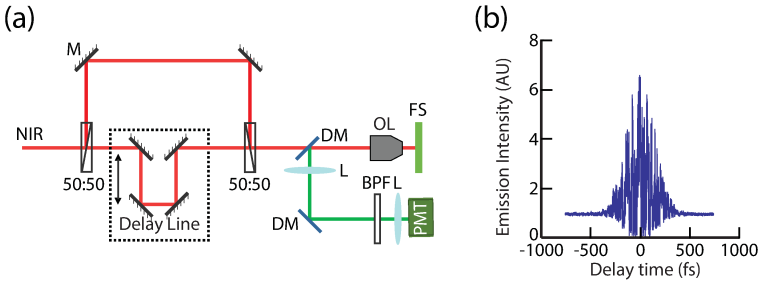

Fig. 7. In the $\lambda_{NIR} = \lambda_{IR}$ limit, the generated fluorescence is an interferometric autocorrelator signal. (a) The experimental setup to study the $\lambda_{NIR} = \lambda_{IR}$ limit. L, lens; 50 : 50, 50 : 50 beam splitter; M, mirror; DM, dichroic mirror; FS, fluorescent sample; OL, objective lens; BPF, band pass filter; PMT, photomultiplier. (b) The fluorescence generated by the setup, shown in a, is an interferometric autocorrelation trace.

Funding

National Institutes of Health (NIH) (BRAIN Initiative U01NS094232, BRAIN Initiative MH111359, NS057198, S10RR029050); National Science Foundation (NSF) (CBET 1445158, ECCS 1405234, ECCS 1507146); Program 973 (2014AA014402); Office of Naval Research (ECE4509); Cymer Corporation; UCSD Center for Brain Activity Mapping (CBAM) (CRES 4-P68).

Acknowledgments

S. Sadegh was supported by the Chancellors Research Excellence Scholarship (CRES 4-P68) from UC San Diego Strategic Planning.

References

1. J. W. Lichtman and J. A. Conchello, "Fluorescence microscopy," Nat. Methods **2**, 910–919 (2005).
2. W. Denk, J. H. Strickler, and W. W. Webb, "Two-photon laser scanning fluorescence microscopy," Science **248**, 73–76 (1990).
3. S. Quentmeier, S. Denicke, and K. H. Gericke, "Two-color two-photon fluorescence laser scanning microscopy," J. Fluoresc. **19**, 1037–1043 (2009).

Optics EXPRESS

4. P. Mahou, M. Zimmerley, K. Loulier, K. S. Matho, G. Labroille, X. Morin, W. Supatto, J. Livet, D. Débarre, and E. Beaurepaire, "Multicolor two-photon tissue imaging by wavelength mixing," Nat. Methods **9**, 815–818 (2012).
5. E. P. Perillo, J. W. Jarrett, Y. L. Liu, A. Hassan, D. C. Fernée, J. R. Goldak, A. Bonteanu, D. J. Spence, H. C. Yeh, and A. K. Dunn, "Two-color multiphoton in vivo imaging with a femtosecond diamond raman laser," Light Sci. Appl. **6**, e17095 (2017).
6. S. Lindek and E. Stelzer, "Resolution improvement by nonconfocal theta microscopy," Opt. Lett. **24**, 1505–1507 (1999).
7. C. Ibáñez-López, I. Escobar, G. Saavedra, and M. Martínez-Corral, "Optical-sectioning improvement in two-color excitation scanning microscopy," Microsc. Res. Tech. **64**, 96–102 (2004).
8. M. H. Yang, M. Abashin, P. A. Saisan, P. Tian, C. G. Ferri, A. Devor, and Y. Fainman, "Non-degenerate 2-photon excitation in scattering medium for fluorescence microscopy," Opt. Express **24**, 30173–30187 (2016).
9. D. R. Miller, J. W. Jarrett, A. M. Hassan, and A. K. Dunn, "Deep tissue imaging with multiphoton fluorescence microscopy," Curr. Opin. Biomed. Eng. **4**, 32–39 (2017).
10. M. O. Cambaliza and C. Saloma, "Advantages of two-color excitation fluorescence microscopy with two confocal excitation beams," Opt. Commun. **184**, 25–35 (2000).
11. C. M. Blanca and C. Saloma, "Two-color excitation fluorescence microscopy through highly scattering media," Appl. Opt. **40**, 2722–2729 (2001).
12. C. Wang, L. Qiao, Z. Mao, Y. Cheng, and Z. Xu, "Reduced deep-tissue image degradation in three-dimensional multiphoton microscopy with concentric two-color two-photon fluorescence excitation," J. Opt. Soc. Am. B **25**, 976–982 (2008).
13. D. Kobat, G. Zhu, and C. Xu, "Background reduction with two-color two-beam multiphoton excitation," in *Biomedical Optics* (Optical Society of America, 2008), p. BMF6.
14. D. Fröhlich and H. Mahr, "Two-photon spectroscopy in anthracene," Phys. Rev. Lett. **16**, 895–897 (1966).
15. P. Monson and W. McClain, "Polarization dependence of the two-photon absorption of tumbling molecules with application to liquid 1-chloronaphthalene and benzene," J. Chem. Phys. **53**, 29–37 (1970).
16. R. A. Negres, J. M. Hales, A. Kobyakov, D. J. Hagan, and E. W. Van Stryland, "Two-photon spectroscopy and analysis with a white-light continuum probe," Opt. Lett. **27**, 270–272 (2002).
17. J. M. Hales, D. J. Hagan, E. W. Van Stryland, K. Schafer, A. Morales, K. D. Belfield, P. Pacher, O. Kwon, E. Zojer, and J.-L. Brédas, "Resonant enhancement of two-photon absorption in substituted fluorene molecules," J. Chem. Phys. **121**, 3152–3160 (2004).
18. D. A. Fishman, C. M. Cirloganu, S. Webster, L. A. Padilha, M. Monroe, D. J. Hagan, and E. W. Van Stryland, "Sensitive mid-infrared detection in wide-bandgap semiconductors using extreme non-degenerate two-photon absorption," Nat. Photonics **5**, 561–565 (2011).
19. K. Podgorski and G. Ranganathan, "Brain heating induced by near-infrared lasers during multiphoton microscopy," J. Neurophysiol. **116**, 1012–1023 (2016).
20. C. Xu and W. W. Webb, "Measurement of two-photon excitation cross sections of molecular fluorophores with data from 690 to 1050 nm," J. Opt. Soc. Am. B **13**, 481–491 (1996).
21. M. Drobizhev, N. S. Makarov, S. E. Tillo, T. E. Hughes, and A. Rebane, "Two-photon absorption properties of fluorescent proteins," Nature Methods **8**, 393–399 (2011).
22. K. D. Belfield, D. J. Hagan, E. W. Van Stryland, K. J. Schafer, and R. A. Negres, "New two-photon absorbing fluorene derivatives: synthesis and nonlinear optical characterization," Org. Lett. **1**, 1575–1578 (1999).
23. B. Xue, C. Katan, J. Bjorgaard, and T. Kobayashi, "Non-degenerate two photon absorption enhancement for laser dyes by precise lock-in detection," AIP Adv. **5**, 127138 (2015).
24. M. Göppert-Mayer, "Über Elementarakte mit zwei Quantensprüngen," Ann. Phys. **401**, 273–294 (1931).
25. R. W. Boyd, *Nonlinear optics* (Elsevier, 2003).
26. H. S. Pattanaik, M. Reichert, J. B. Khurgin, D. J. Hagan, and E. W. Van Stryland, "Enhancement of two-photon absorption in quantum wells for extremely nondegenerate photon pairs," IEEE J. Quantum Electron. **52**, 1–14 (2016).
27. J. C. M. Diels, J. J. Fontaine, I. C. McMichael, and F. Simoni, "Control and measurement of ultrashort pulse shapes (in amplitude and phase) with femtosecond accuracy," Appl. Opt. **24**, 1270–1282 (1985).